Electronic Supplementary Information

From Vanadium Slag to Multi-Cations Intercalated $V_2O_5 \cdot nH_2O$: Low-Cost Direct Synthesis and High-Performance Aqueous Battery Application

Dong Chen,‡[a] Haoliang Chen,‡[a] Cheng-Feng Du,[b] Lin Liu,[a] Hongbo Geng,[c] Hong Yu,*[b] and Xianhong Rui*[a]

a. School of Materials and Energy, Guangdong University of Technology, Guangzhou 510006, China. E-mail: xhrui@gdut.edu.cn

b. Center of Advanced Lubrication and Seal Materials Northwestern Polytechnical University, Xi'an 710072, China. E-mail: yh@nwpu.edu.cn

c. School of Materials Engineering Changshu Institute of Technology Changshu, Jiangsu 215500, China.

‡ D. Chen and H. Chen contributed equally to this work.

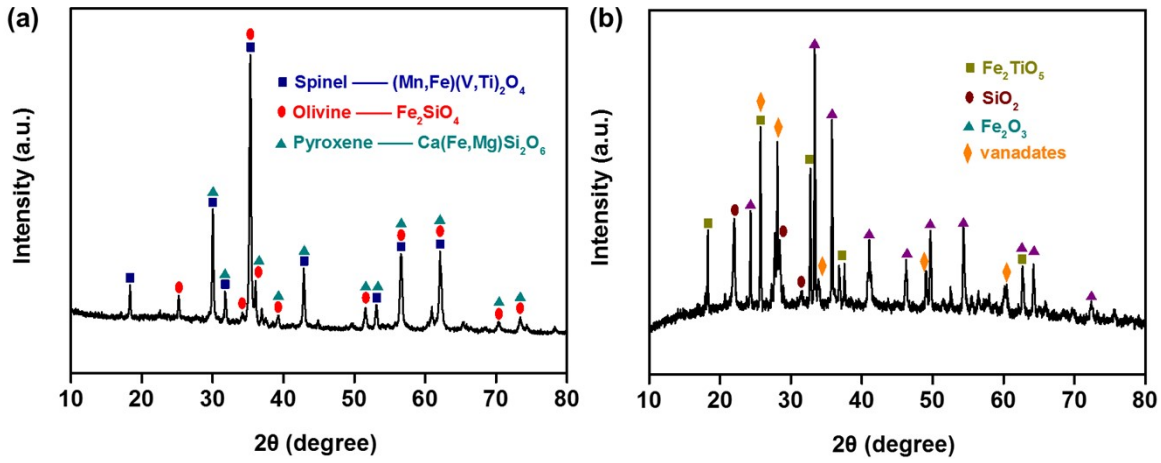

Fig. S1. XRD patterns of (a) original and (b) roasting vanadium slag.

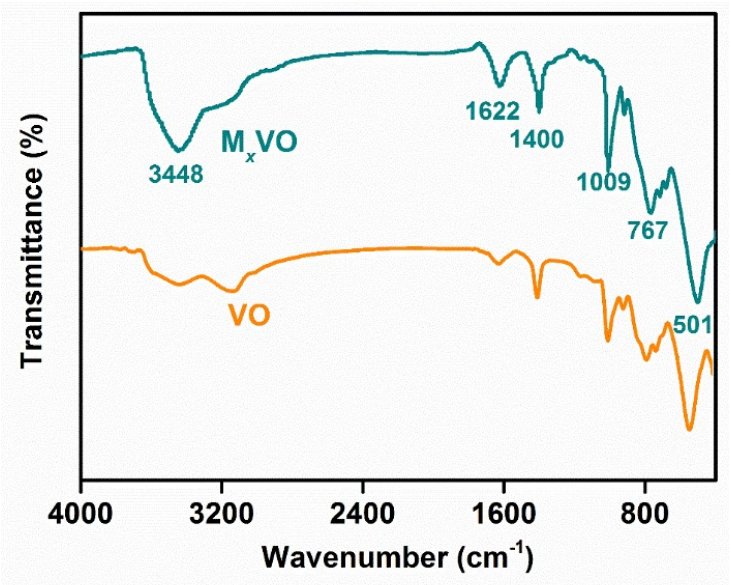

Fig. S2. FTIR spectrum of M_xVO and VO.

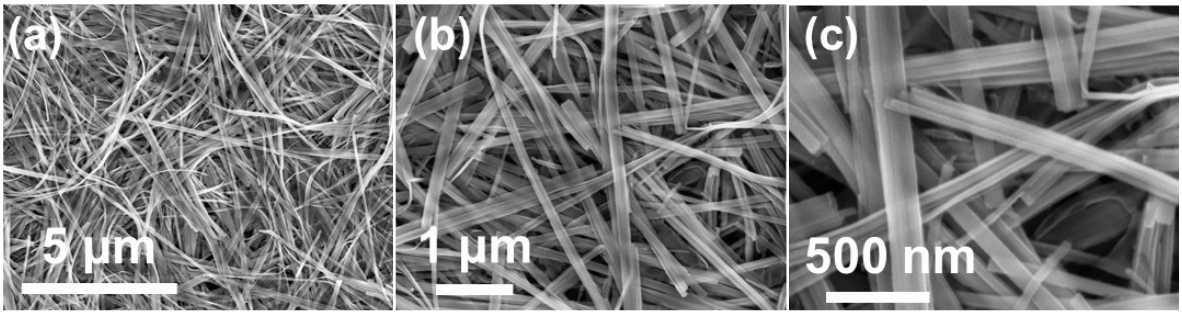

Fig. S3. SEM images of VO.

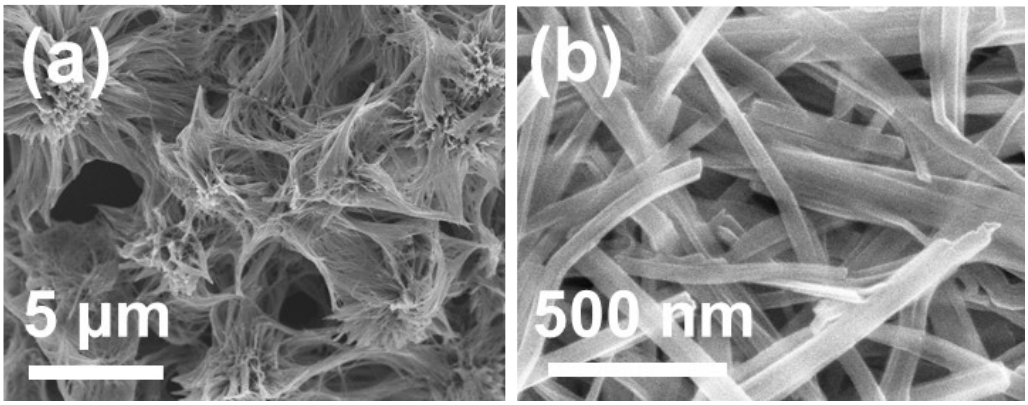

Fig. S4. SEM images of M_xVO.

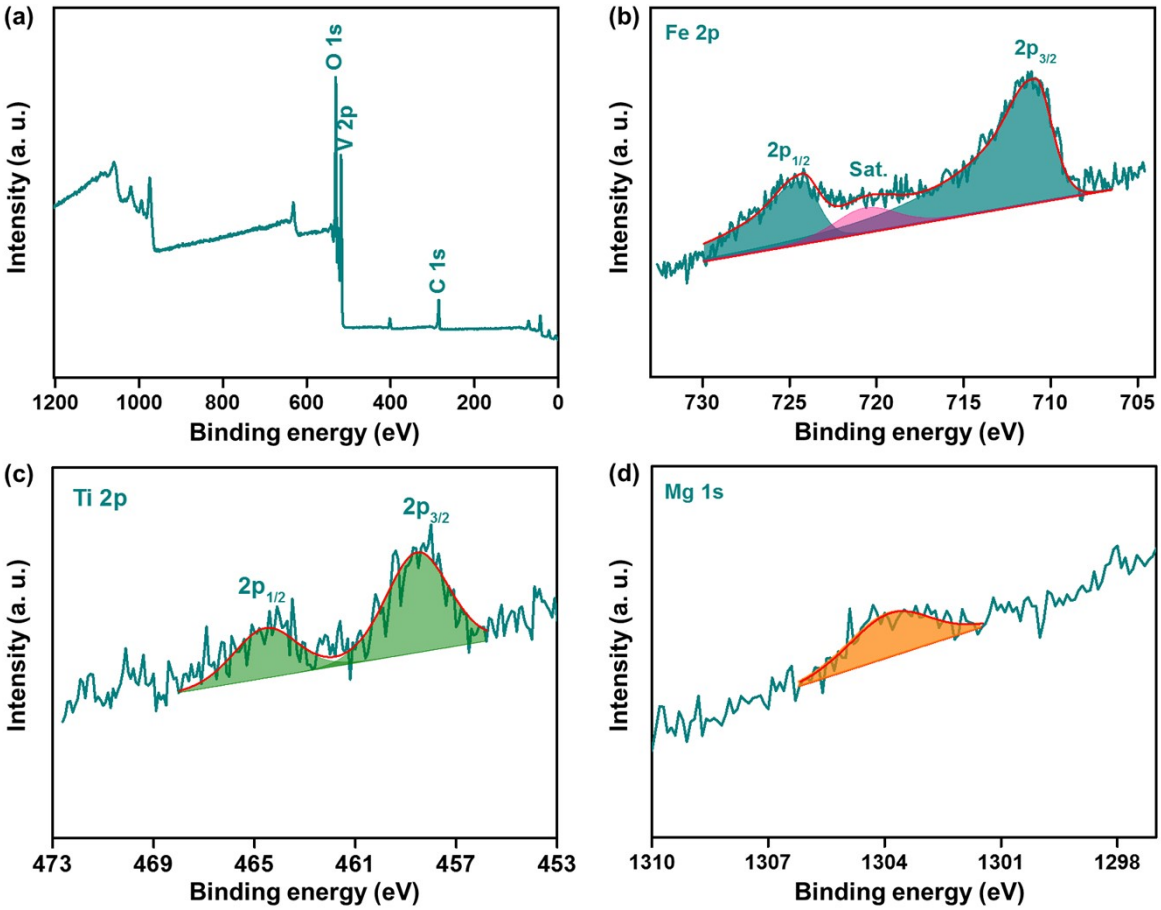

Fig. S5. XPS spectrum of M_xVO: (a) the survey scan spectrum and (b-d) high resolution spectrum of (b) Fe 2p, (c) Ti 2p and (d) Mg 1s.

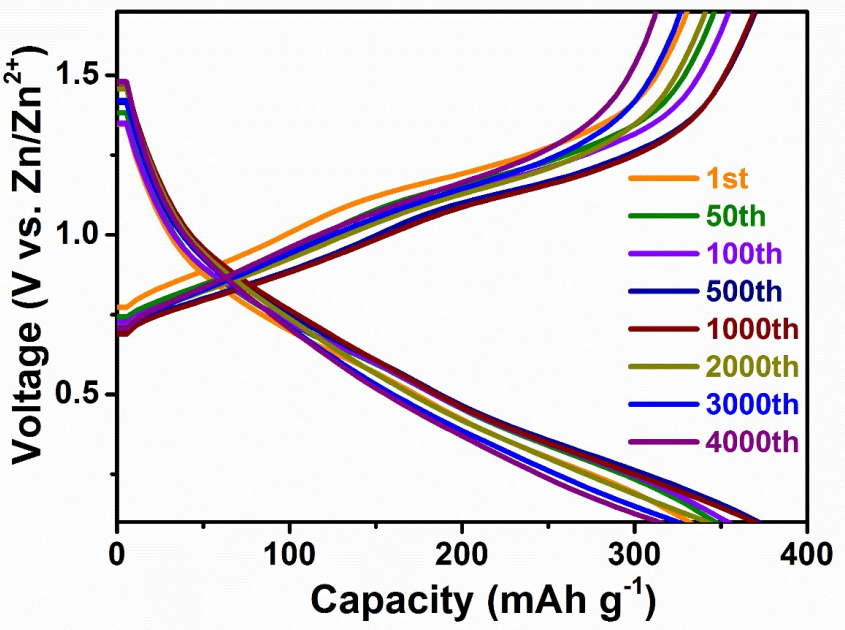

Fig. S6. Galvanostatic discharge and charge profiles of the M_xVO cathode at 20 A g^{-1}, whose shape are well maintained with good reversibility during long-term cycling process, illustrating an outstanding cycle stability.

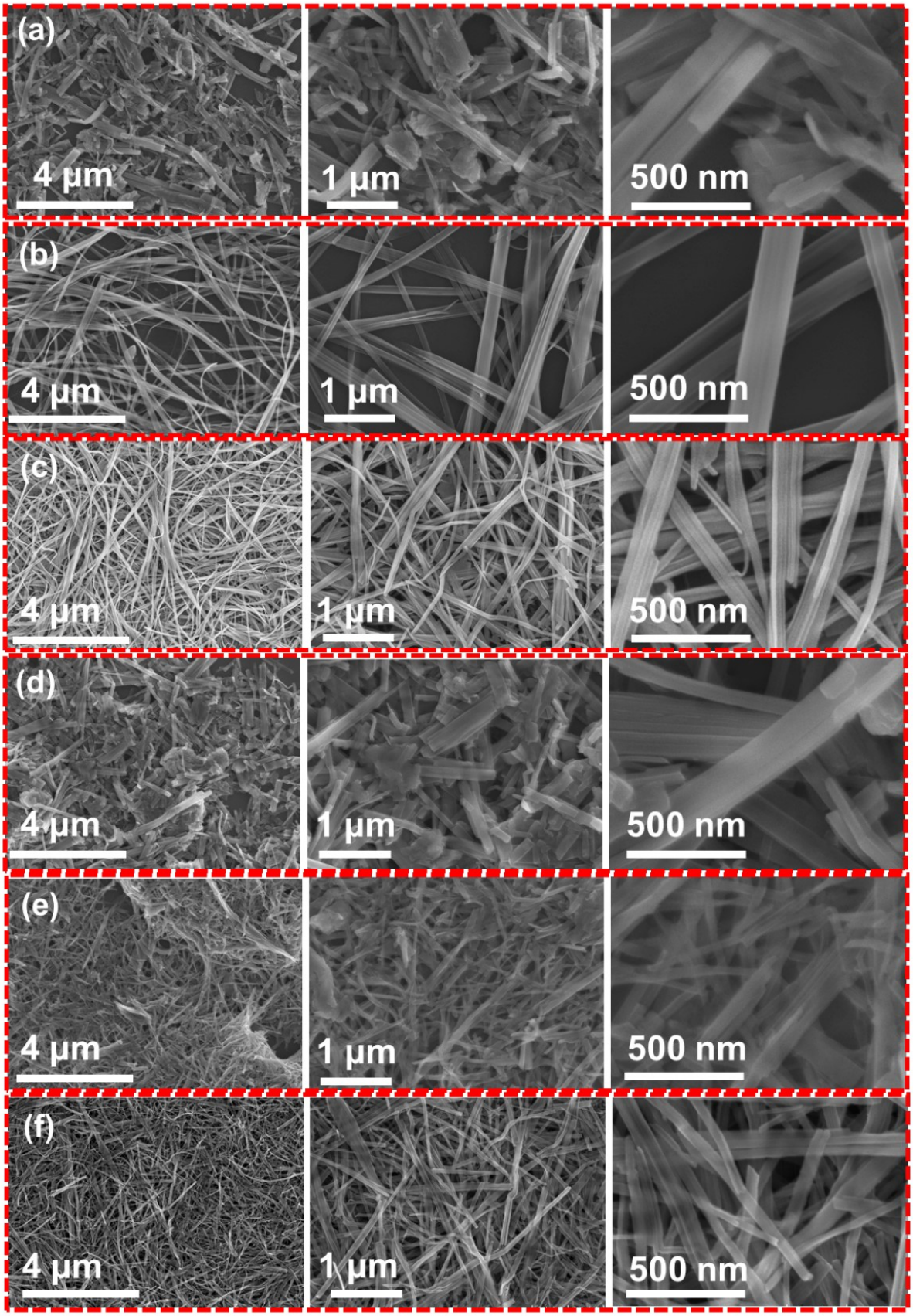

Fig. S7. SEM images of (a) Ti_xVO, (b) Mg_xVO, (c) Fe_xVO, (d) $(Mg,Ti)_xVO$, (e) $(Fe,Ti)_xVO$ and (f) $(Fe,Mg)_xVO$.

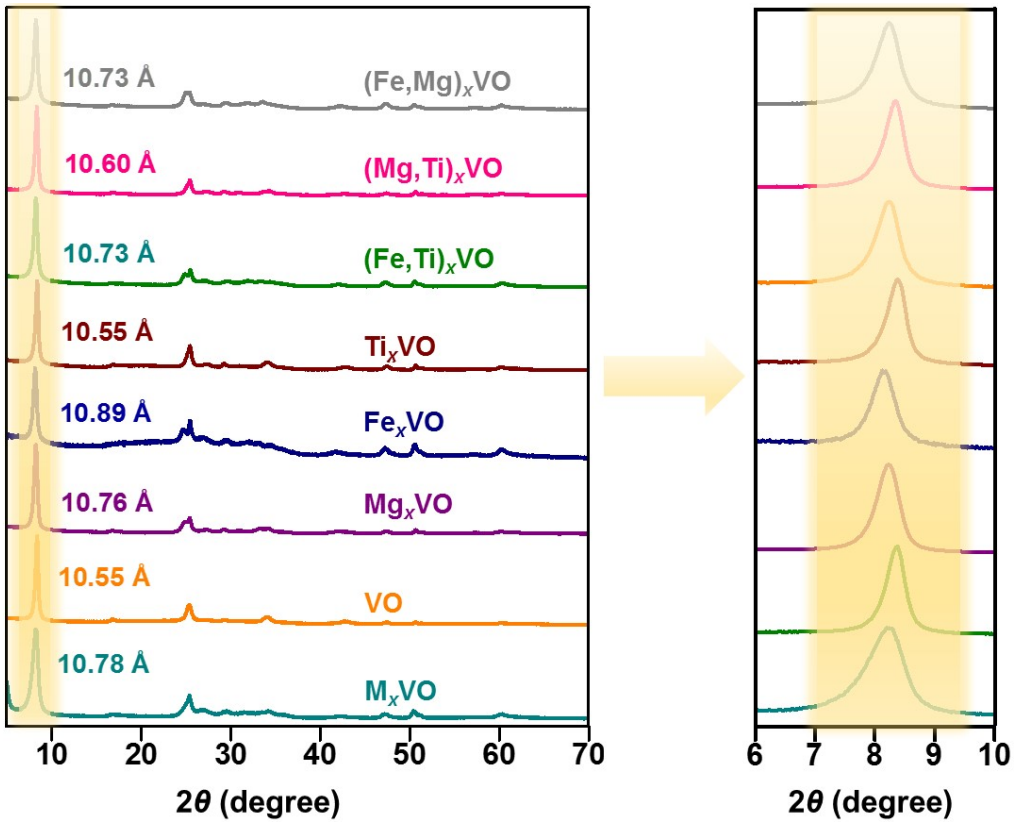

Fig. S8. XRD patterns of diverse hydrated vanadates.

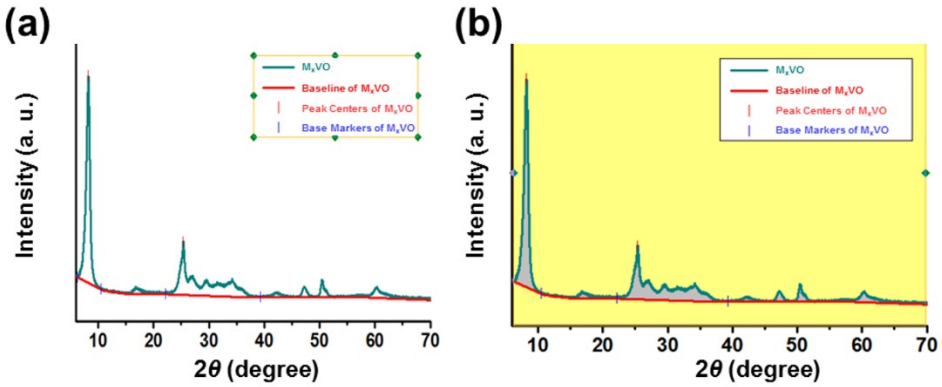

Fig. S9. Calculation process of crystallinity for the M_xVO. (a) Baseline adjustment, and (b) the total area under the peaks.

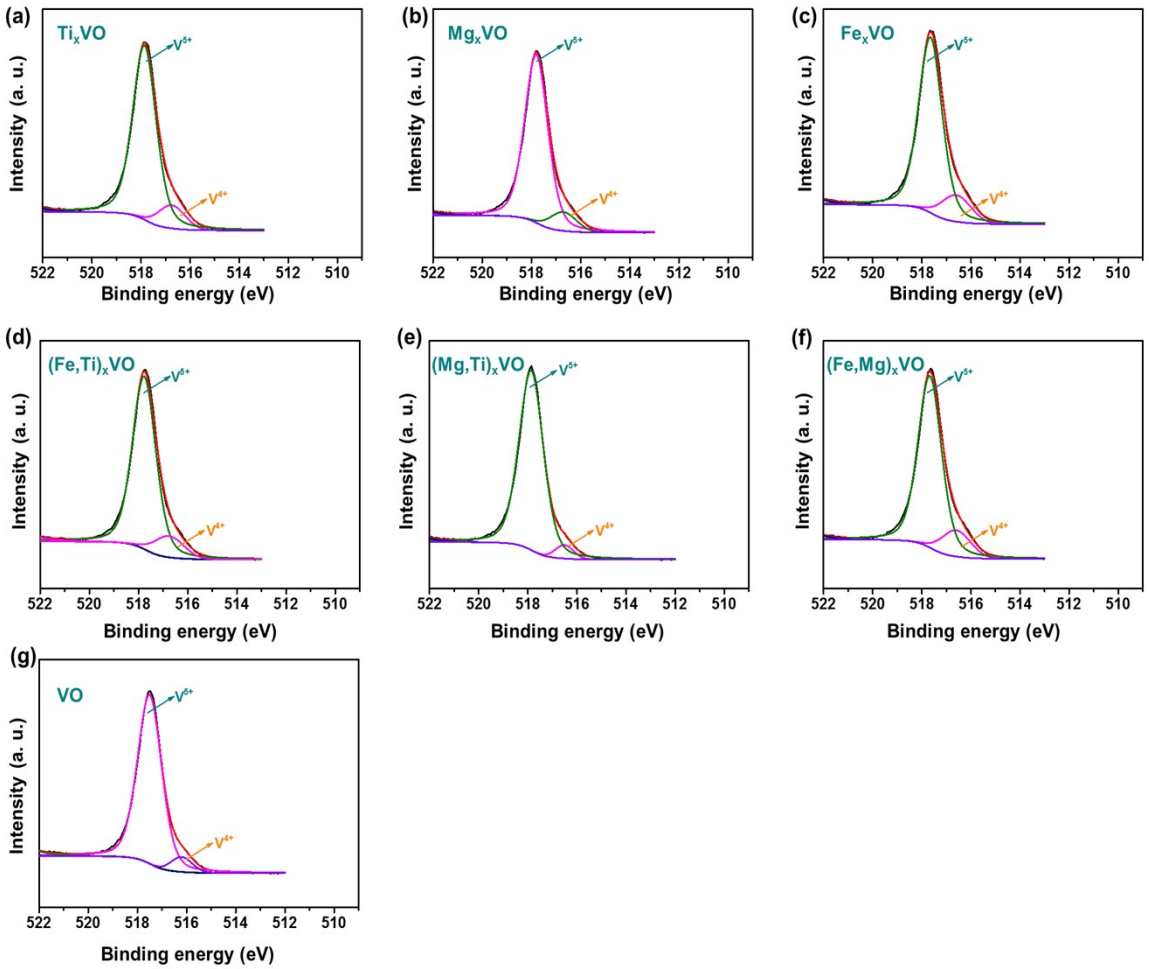

Fig. S10. XPS spectra of V $2p_{3/2}$ region for (a) Ti_xVO, (b) Mg_xVO, (c) Fe_xVO, (d) $(Fe,Ti)_xVO$, (e) $(Mg,Ti)_xVO$, (f) $(Fe,Mg)_xVO$, and (g) VO.

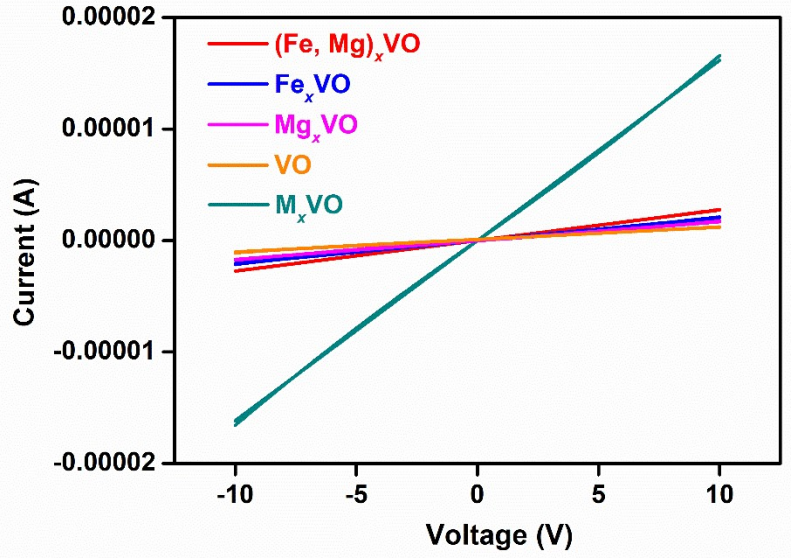

Fig. S11. Electrical conductivity of $(Fe, Mg)_xVO$, Fe_xVO, Mg_xVO, VO and M_xVO.

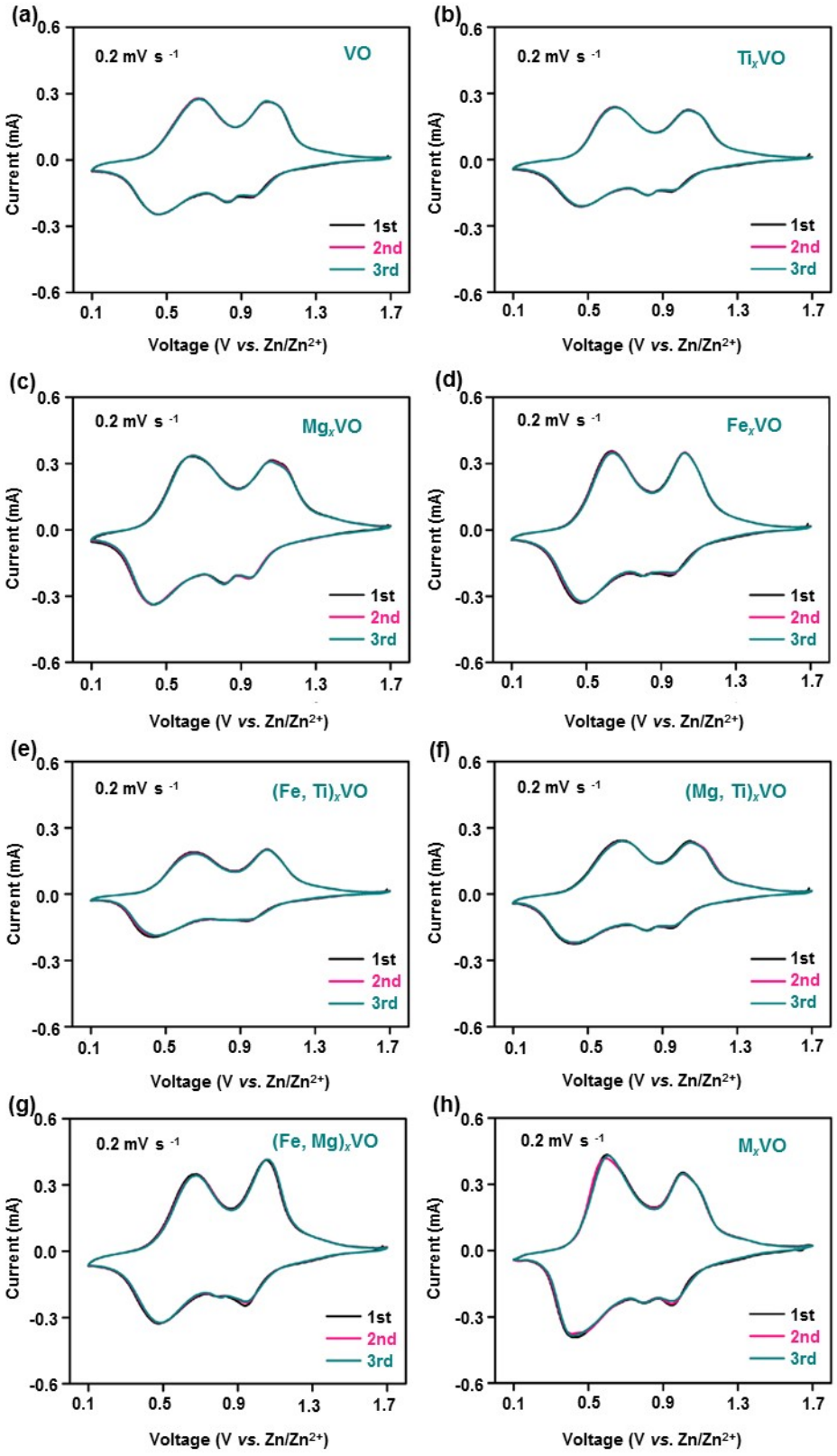

Fig. S12. CV curves at 0.2 mV s^{-1} in the potential range of 0.1-1.7V *vs* Zn/Zn^{2+} of (a) VO, (b) Ti_xVO, (c) Mg_xVO, (d) Fe_xVO, (e) $(Fe,Ti)_xVO$, (f) $(Mg,Ti)_xVO$, (g) $(Fe,Mg)_xVO$ and (h) M_xVO.

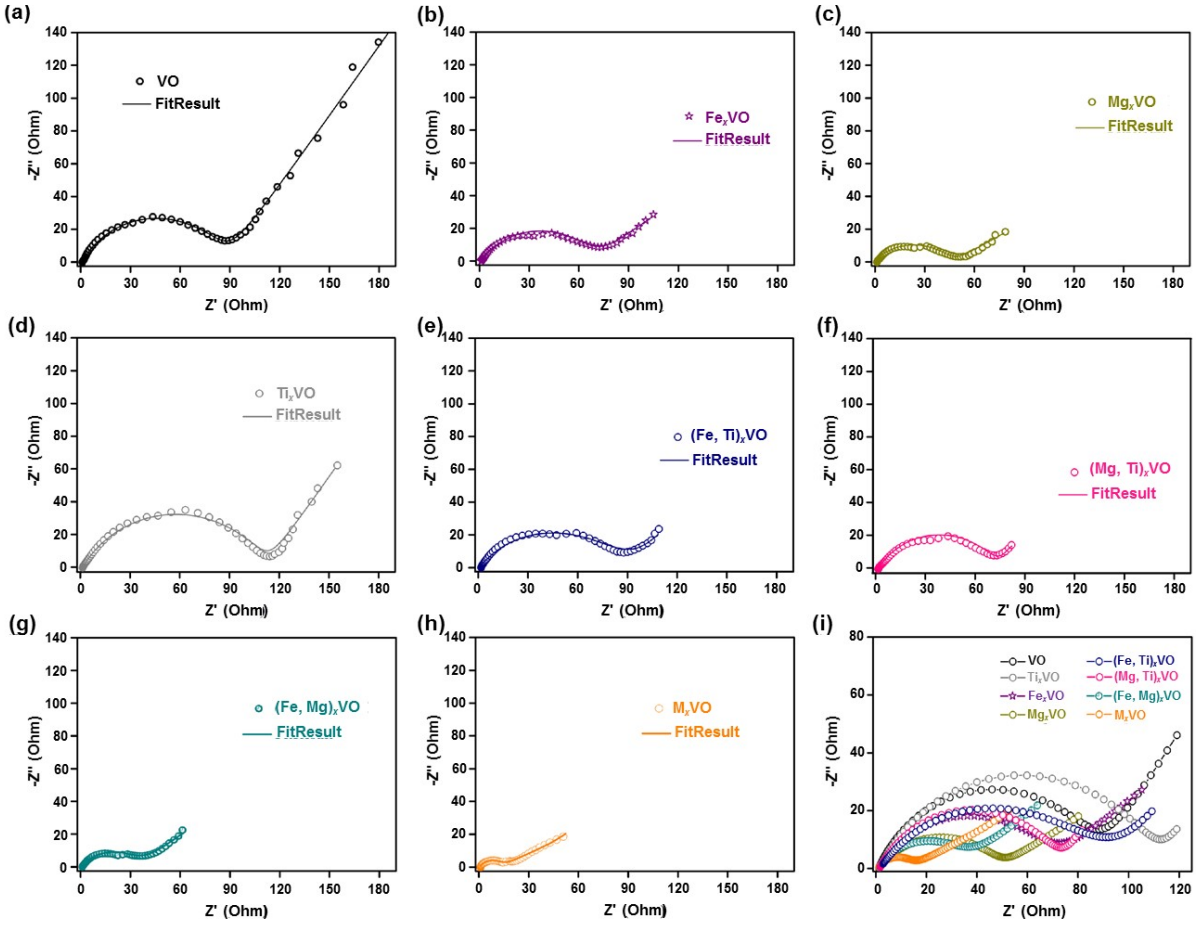

Fig. S13. A comparison of the electrochemical impedance spectra (EIS) in the pristine state of M_xVO electrode and as-simulated hydrated vanadate electrodes.

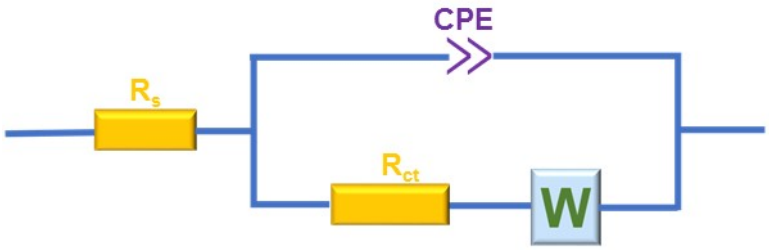

Fig. S14. The equivalent circuit used for fitting the above EIS curves (Fig. S11), in which R_s is bulk resistance, R_{ct} is charge transfer resistance, CPE is constant phase element, and W is Warburg impedance.

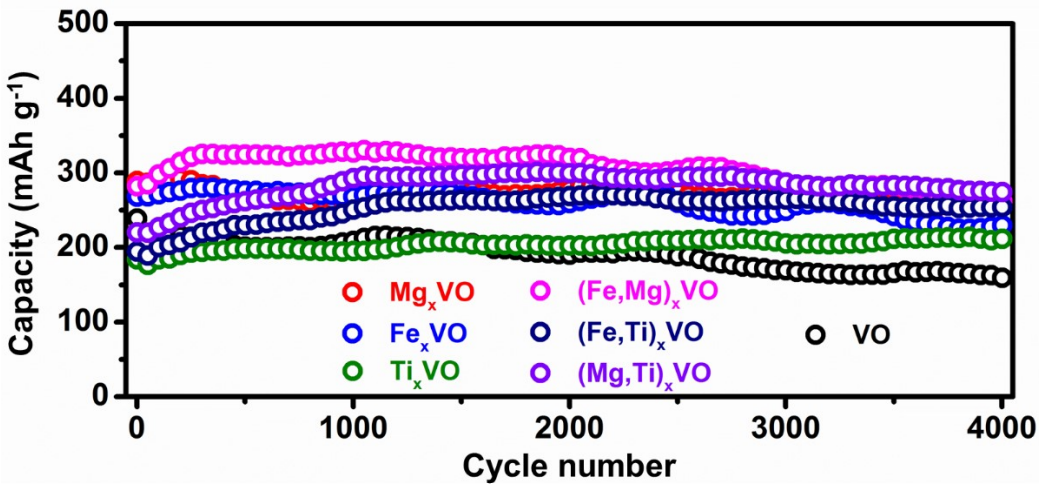

Fig. S15. Long-term cycling performance at 20 A g^{-1} of the as-simulated cations pre-intercalated hydrated vanadate samples.

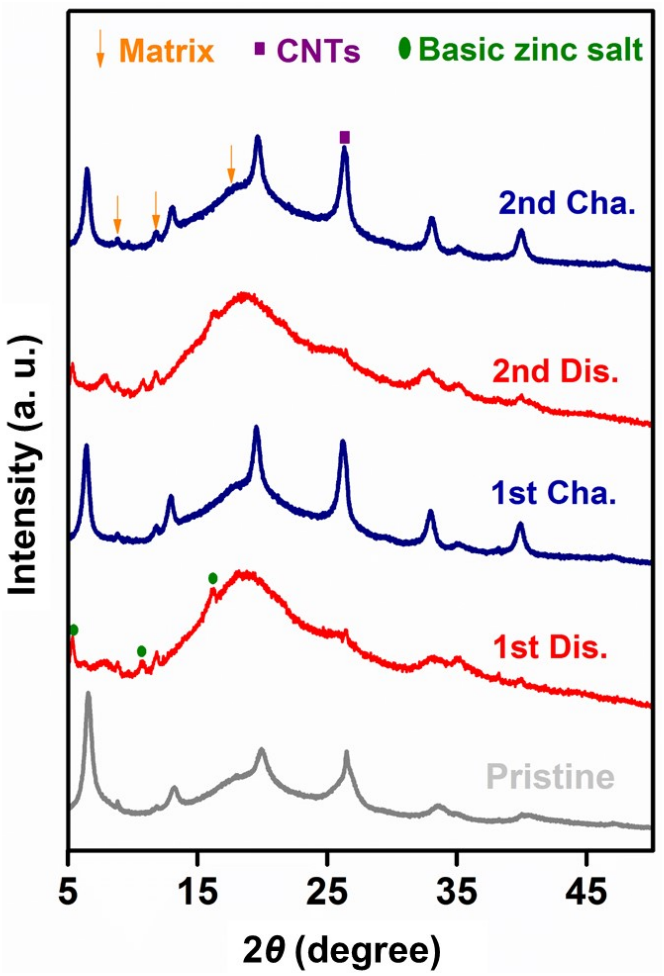

Fig. S16. The XRD patterns of M_xVO electrode at different states.

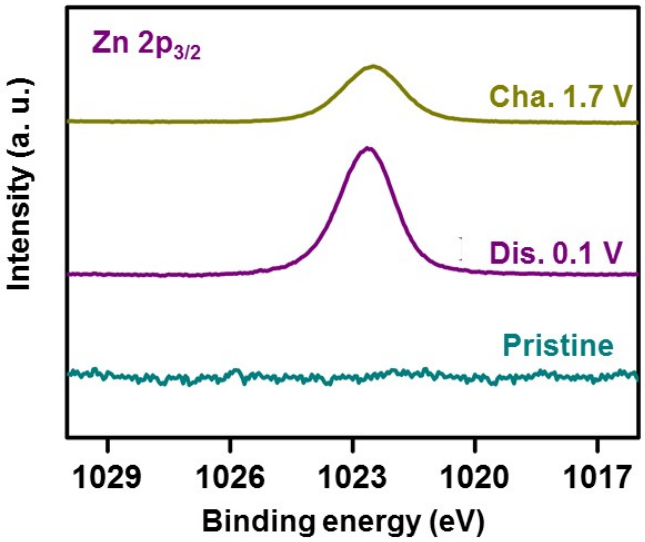

Fig. S17. High-resolution Zn 2p XPS spectra of M_xVO electrode at pristine, fully discharged and fully charged states.

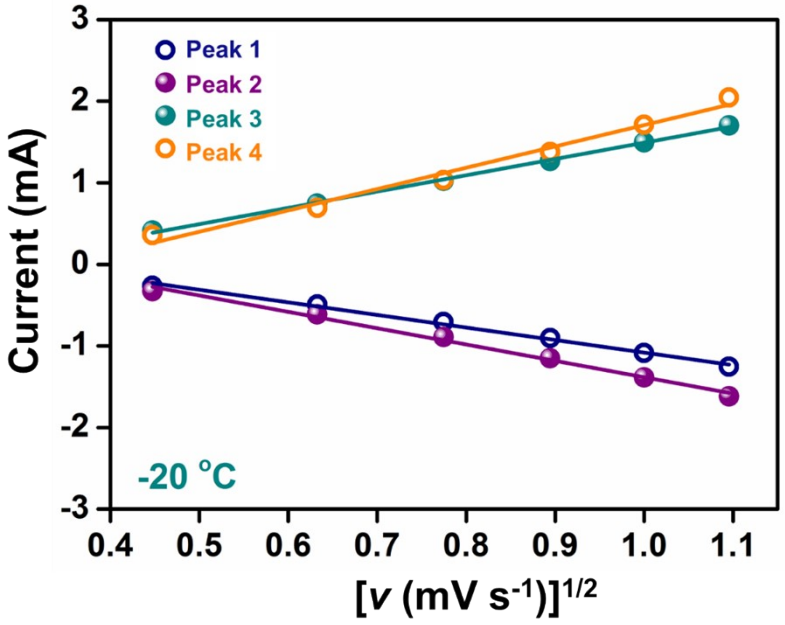

Fig. S18. I (current density) *vs.* $v^{1/2}$ (scan rate) fitting plots based on four peaks in Fig. 5b.

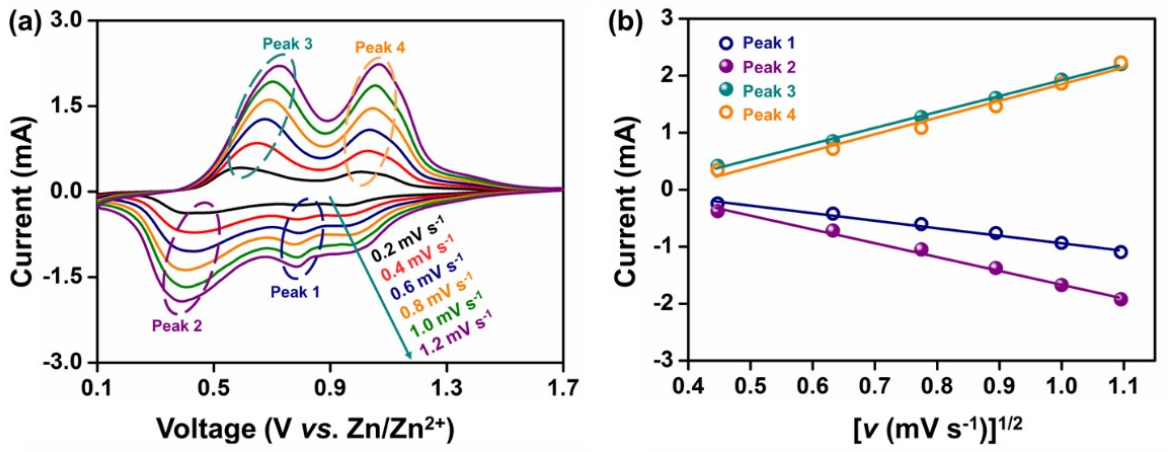

Fig. S19 (a) CV curves at different scan rates in the potential range of 0.1-1.7 V vs. Zn/Zn^{2+} at room temperature, (b) I (current density) vs. $v^{1/2}$ (scan rate) fitting plots based on four peaks.

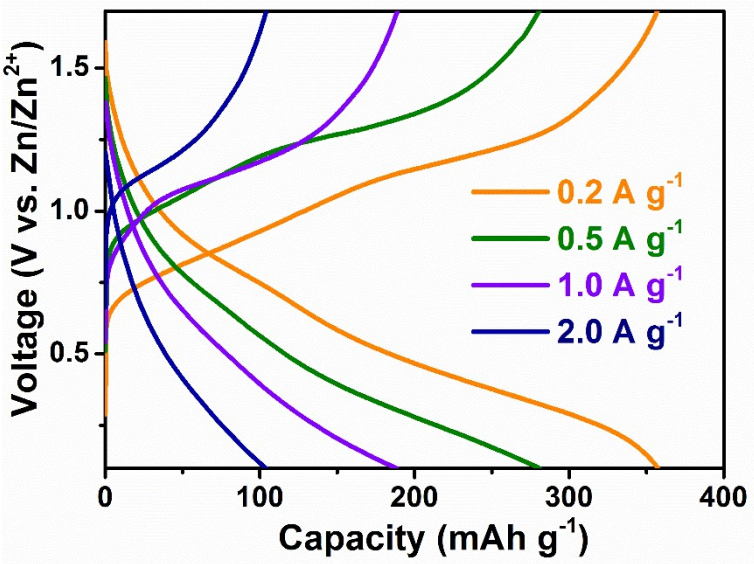

Fig. S20. Galvanostatic discharge and charge profiles of the pouch cell at various current densities.

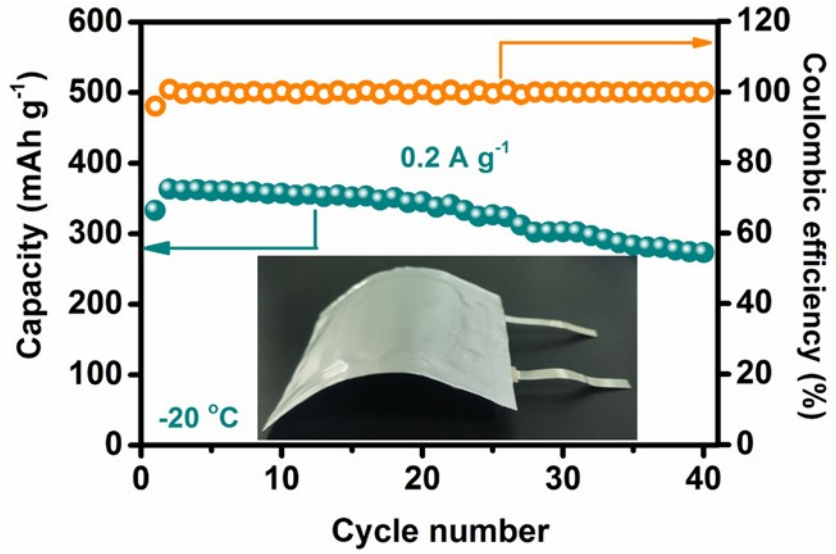

Fig. S21. Cycling performance at 0.2 A g^{-1} of Zn/M_xVO pouch cell under bending.

Table S1. The chemical composition of vanadium slag.

Analyte	Concentration (%)	Analyte	Concentration (%)
Fe	12.954	Al	0.995
V	4.474	Ca	0.765
Ti	3.209	Mg	0.729
Si	3.105	O	70.819
Mn	2.642	Others	0.308

Table S2. Qualitative analysis of M_xVO by XRF.

Analyte	V	Fe	Ti	Mg	O
Concentration (%)	22.739	0.220	0.047	0.029	76.965

Table S3. Quantitative analysis of M_xVO by ICP-AES.

Analyte	M (mg/kg)	V (mg/kg)	M/V (mole ratio)
Fe	9706.0		0.016
Ti	1444.6	536645.5	0.003
Mg	289.0		0.001

Table S4. A comparison of electrochemical performance of M_xVO with that of the currently representative vanadium-based cathodes.

Cathode	Cycling stability	Rate performance
M_xVO	**262 mAh g^{-1} @ 20 A g^{-1}, 4000 cycles (30 °C)** **230 mAh g^{-1} @ 10 A g^{-1}, 1000 cycles (-20 °C)**	**203 mAh g^{-1} @ 100 A g^{-1} (30 °C)** **121 mAh g^{-1} @ 50 A g^{-1} (-20 °C)**
MnVOH[1]	260 mAh g^{-1} @ 4 A g^{-1}, 2000 cycles	214 mAh g^{-1} @ 8 A g^{-1}
AlVOH[2]	236 mAh g^{-1} @ 4 A g^{-1}, 3000 cycles	195 mAh g^{-1} @ 8 A g^{-1}
VO_2[3]	250 mAh g^{-1} @ 2 A g^{-1}, 300 cycles	171 mAh g^{-1} @ 51.2 A g^{-1}
$VN_{0.9}O_{0.15}$[4]	139 mAh g^{-1} @ 4 A g^{-1}, 1500 cycles	124 mAh g^{-1} @ 102.4 A g^{-1}
ZVO[5]	214 mAh g^{-1} @ 10 A g^{-1}, 20000 cycles	265 mAh g^{-1} @ 10 A g^{-1}
$(Na,Mn)V_8O_{20}\cdot nH_2O$[6]	128 mAh g^{-1} @ 4 A g^{-1}, 1000 cycles	146 mAh g^{-1} @ 8 A g^{-1}
$Ag_{0.4}V_2O_5$[7]	144 mAh g^{-1} @ 20 A g^{-1}, 4000 cycles	180 mAh g^{-1} @ 2 A g^{-1}
V_2O_5[8]	169 mAh g^{-1} @ 10 A g^{-1}, 500 cycles	219 mAh g^{-1} @ 10 A g^{-1}
$Li_xV_2O_5\cdot nH_2O$[9]	192 mAh g^{-1} @ 10 A g^{-1}, 1000 cycles	170 mAh g^{-1} @ 10 A g^{-1}
V_6O_{13}[10]	230 mAh g^{-1} @ 4 A g^{-1}, 2000 cycles	145 mAh g^{-1} @ 24 A g^{-1}
$Mg_xV_2O_5\cdot nH_2O$[11]	90 mAh g^{-1} @ 5 A g^{-1}, 2000 cycles	81 mAh g^{-1} @ 5 A g^{-1}
$NaV_3O_8\cdot 1.5H_2O$[12]	135 mAh g^{-1} @ 4 A g^{-1}, 1000 cycles	165 mAh g^{-1} @ 4 A g^{-1}
$Na_{0.33}V_2O_5$[13]	218 mAh g^{-1} @ 1 A g^{-1}, 1000 cycles	96 mAh g^{-1} @ 2 A g^{-1}
VS_4@rGO[14]	168 mAh g^{-1} @ 1 A g^{-1}, 165 cycles	200 mAh g^{-1} @ 2 A g^{-1}
$Zn_2V_2O_7$[15]	138 mAh g^{-1} @ 4 A g^{-1}, 1000 cycles	170 mAh g^{-1} @ 4.4 A g^{-1}
$V_2O_5\cdot nH_2O$[16]	200 mAh g^{-1} @ 6 A g^{-1}, 900 cycles	248 mAh g^{-1} @ 30 A g^{-1}
VO_2[17]	86 mAh g^{-1} @ 3 A g^{-1}, 5000 cycles	72 mAh g^{-1} @ 5 A g^{-1}
$(NH_4)_2V_{10}O_{25}\cdot 8H_2O$[18]	90 mAh g^{-1} @ 5 A g^{-1}, 5000 cycles	124 mAh g^{-1} @ 5 A g^{-1}
C-KVO|O_d[19]	245 mAh g^{-1} @ 3 A g^{-1}, 1000 cycles	166 mAh g^{-1} @ 20 A g^{-1}
PEDOT-$NH_4V_3O_8$[20]	161 mAh g^{-1} @ 10 A g^{-1}, 5000 cycles	164 mAh g^{-1} @ 10 A g^{-1}
P-V_2O_3@C[21]	158 mAh g^{-1} @ 5 A g^{-1}, 4000 cycles	228 mAh g^{-1} @ 2 A g^{-1}

Table S5. Quantitative analysis of hydrothermal solutions by ICP-AES (mg/L).

Analyte	1	2	3	
Fe	38.65	24.21	29.94	30.93
Ti	4.85	5.14	4.78	4.92
Mg	170.35	203.78	185.48	186.54
V	1518.59	1691.87	1599.20	1603.22

Table S6. A comparasion of the crystallinity.

Sample	VO	Ti_xVO	Mg_xVO	Fe_xVO	$(Fe,Ti)_xVO$	$(Mg,Ti)_xVO$	$(Fe,Mg)_xVO$	M_xVO
Crystallinity (%)	99.91	99.88	99.92	99.95	99.90	99.88	99.91	99.89

Table S7. A comparasion of the average valence state of V.

Sample	VO	Ti_xVO	Mg_xVO	Fe_xVO	$(Fe,Ti)_xVO$	$(Mg,Ti)_xVO$	$(Fe,Mg)_xVO$	M_xVO
Average valence state	4.93	4.89	4.90	4.86	4.88	4.94	4.86	4.92

Table S8. Simulated parameters from EIS curves in Fig. S12 using equivalent circuit.

Sample	R_s (Ω)	CPE (μF)	R_{ct} (Ω)
VO	1	7	88
Ti_xVO	1	7	112
Mg_xVO	1	5	48
Fe_xVO	1	6	69
$(Fe,Ti)_xVO$	2	6	80
$(Mg,Ti)_xVO$	2	6	72
$(Fe,Mg)_xVO$	1	6	35
M_xVO	1	6	13

Table S9. Comparasion of the diffusion coefficient (D_{Zn}^{2+}) with some reported electrode materials.

Electrode Materials	D_{Zn}^{2+}(cm^{-2} s^{-1})	Ref.
M_xVO	$10^{-6} \sim 10^{-8}$ (-20 °C)	This work
$K_{1.14}(VO)_{3.33}[Fe(CN)_6]_2 \cdot 6.8H_2O$	$10^{-9} \sim 10^{-14}$	22
$Mn_{0.15}V_2O_5 \cdot nH_2O$	$10^{-10} \sim 10^{-12}$	23
Graphene Scroll Coated α-MnO_2	$10^{-12} \sim 10^{-17}$	24
MnO_2 nanospheres	$10^{-12} \sim 10^{-15}$	25
La-Ca co-doped ε-MnO_2	$10^{-8} \sim 10^{-9}$	26
(PANI)-intercalated V_2O_5	$10^{-10} \sim 10^{-12}$	27

References

1 C. Liu, Z. Neale, J. Zheng, X. Jia, J. Huang, M. Yan, M. Tian, M. Wang, J. Yang and G. Cao, *Energy Environ. Sci.*, 2019, **12**, 2273-2285.

2 J. Zheng, C. Liu, M. Tian, X. Jia, E. Jahrman, G. Seidler, S. Zhang, Y. Liu, Y. Zhang, C. Meng and G. Cao, *Nano Energy*, 2020, **70**, 104519.

3 J. Ding, Z. Du, L. Gu, B. Li, L. Wang, S. Wang, Y. Gong and S. Yang, *Adv. Mater.*, 2018, **30**, 1800762.

4 J. Ding, Z. Du, B. Li, L. Wang, S. Wang, Y. Gong and S. Yang, *Adv. Mater.*, 2019, **31**, 1904369.

5 L. Wang, K.W. Huang, J. Chen and J. Zheng, *Sci. Adv.*, 2019, **5**, eaax4279.

6 M. Du, C. Liu, F. Zhang, W. Dong, X. Zhang, Y. Sang, J.-J. Wang, Y. Guo, H. Liu and S. Wang, *Adv. Sci.*, 2020, **7**, 2000083.

7 L. Shan, Y. Yang, W. Zhang, H. Chen, G. Fang, J. Zhou and S. Liang, *Energy Storage Mater.*, 2019, **18**, 10-14.

8 Y. Li, Z. Huang, P. K. Kalambate, Y. Zhong, Z. Huang, M. Xie, Y. Shen and Y. Huang, *Nano Energy*, 2019, **60**, 752-759.

9 Y. Yang, Y. Tang, G. Fang, L. Shan, J. Guo, W. Zhang, C. Wang, L. Wang, J. Zhou and S. Liang, *Energy Environ. Sci.*, 2018, **11**, 3157-3162.

10 J. Shin, D. S. Choi, H. J. Lee, Y. Jung and J. W. Choi, *Adv. Energy Mater.*, 2019, **9**, 1900083.

11 F. Ming, H. Liang, Y. Lei, S. Kandambeth, M. Eddaoudi and H. N. Alshareef, *ACS Energy Lett.*, 2018, **3**, 2602-2609.

12 F. Wan, L. Zhang, X. Dai, X. Wang, Z. Niu and J. Chen, *Nat. Commun.*, 2018, **9**, 1656.

13 P. He, G. Zhang, X. Liao, M. Yan, X. Xu, Q. An, J. Liu and L. Mai, *Adv. Energy Mater.*, 2018, **8**, 1702463.

14 H. Qin, Z. Yang, L. Chen, X. Chen and L. Wang, *J. Mater. Chem. A*, 2018, **6**, 23757-23765.

15 B. Sambandam, V. Soundharrajan, S. Kim, M. H. Alfaruqi, J. Jo, S. Kim, V. Mathew, Y.-k. Sun and J. Kim, *J. Mater. Chem. A*, 2018, **6**, 3850-3856.

16 M. Yan, P. He, Y. Chen, S. Wang, Q. Wei, K. Zhao, X. Xu, Q. An, Y. Shuang, Y. Shao, K. T. Mueller, L. Mai, J. Liu and J. Yang, *Adv. Mater.*, 2018, **30**, 1703725.

17 L. Chen, Y. Ruan, G. Zhang, Q. Wei, Y. Jiang, T. Xiong, P. He, W. Yang, M. Yan, Q. An and L. Mai, *Chem. Mater.*, 2019, **31**, 699-706.

18 T. Wei, Q. Li, G. Yang and C. Wang, *J. Mater. Chem. A*, 2018, **6**, 20402-20410.

19 T. Wei, Q. Li, G. Yang and C. Wang, *J. Alloy. Comp.*, 2020, **827**, 154276.

20 D. Bin, W. Huo, Y. Yuan, J. Huang, Y. Liu, Y. Zhang, F. Dong, Y. Wang and Y. Xia, *Chem*, 2020, **6**, 968-984.

21 Y. Ding, Y. Peng, S. Chen, X. Zhang, Z. Li, L. Zhu, L. Mo and L. Hu, *ACS Appl. Mater. Interfaces*, 2019, **11**, 44109-44117.

22 F. Wang, Y. Li, W. Zhu, X. Ge, H. Cui, K. Feng, S. Liu and X. Yang, *ACS Appl. Mater. Interfaces*, 2021, **13**, 34468-34476.

23 H. Geng, M. Cheng, B. Wang, Y. Yang, Y. Zhang and C. Li, *Adv. Funct. Mater.*, 2020, **30**, 1907684.

24 B. Wu, G. Zhang, M. Yan, T. Xiong, P. He, L. He, X. Xu and L. Q. Mai, *Small*, 2018, **14**, 1703850.

25 J. Wang, J. Wang, H. Liu, C. Wei and F. Kang, *J. Mater. Chem. A*, 2019, **7**, 13727-13735.

26 M. Zhang, W. Wu, J. Luo, H. Zhang, J. Liu, X. Liu, Y. Yang and X. Lu, *J. Mater. Chem. A*, 2020, **8**, 11642-11648.

27 S. Liu, H. Zhu, B. Zhang, G. Li, H. Zhu, Y. Ren, H. Geng, Y. Yang, Q. Liu and C.C. Li, *Adv. Mater.*, 2020, **32**, 2001113.